1.1 Introduction

"Quantum Materials" emerged as one of the most vivacious areas across the landscape of present research in physics. These materials are very efficient to apply in faster quantum computing, memory devices, information technology, and spintronics devices. Such materials are advantageous over classical or nanostructured materials as they are associated with novel entanglements or topological properties. The topological properties signify the word topology, which is a branch of mathematics associated with another mathematical term genus number representing the number of holes in the surface [1], [2]. The Noble Prize in theoretical condensed matter physics was given to David J. Thouless, F. Duncan M. Haldane, and J. Michael Kosterlitz in 2016 for their theoretical work on topological phase transition and topological phases of matter. The perception of topological matters initiated by the concept of quantum Hall effect (QHE) [3], [4] in a two-dimensional (2-D) electron gas system under the application of an out-of-plane magnetic field, which is a quantum version of the classical Hall phenomena. As a result of the quantum Hall effect (QHE), a novel state of quantum matter with a conducting edge state and an insulating bulk containing localized electrons has been discovered. However, similar phenomena can be realized as quantum spin Hall effect (QSHE) [5], [6], [7] in two-dimensional or three-dimensional (3-D) topologically protected materials without application of external magnetic field, driven by internal spin-orbit coupling (SOC) [8], [9] of the material protected by time-reversal symmetry (TRS) [4], [10]. Certain materials like topological insulators (TIs) [4], [11], Weyl semimetals (WSMs) [12]–[15] and Skyrmions [16] are the most studied quantum materials that exist with strong SOC under TRS protection. Among them, the 2-D or 3-D TIs are the types of materials with insulating bulk and the conducting edge state or surface state driven by strong SOC protected by the TRS. However, the WSMs might be considered as 3-D analogue of Graphene upon breaking either time-reversal

symmetry or inversion symmetry. Additionally, unlike the topological surface state (TSS), the Fermi surface of the surface state of WSMs represents an open line termed the Fermi Arc linking the surface projections of Weyl nodes [17]. Moreover, the Skyrmions are topologically protected spin configurations observed in non-centrosymmetric non-trivial heli-magnets exhibiting particle-like characteristics that provide enormous stability even at nanoscale at a particular temperature range under very small perturbation [18]–[20]. The Skyrmions are basically the potential carrier of information possibly be applied in future high-density data storage devices, ultrafast spintronics devices and microwave devices. The present thesis is based upon the detailed investigation of magnetic and transport properties of such bulk and heterostructured magnetic topological insulators and magnetic Weyl semimetals displaying Skyrmion-like exotic spin texture. The unique properties of these materials prepare a good podium for understanding interesting physics and can potentially be used in future technological applications [4]. Therefore, the study of these quantum materials provides us the best logical corridor to connect the most important key components of science and technology, which are matter, energy and information.

1.2 Topology in Topological Phase

As we have discussed earlier, quantum materials are associated with the topological property, which originates with the concept of topology. Topology is a mathematical perception, according to which the doughnut and the coffee mug shown in Figure 1.1 (a) are identical by means they can be transformed into one another through smooth deformation without tearing or gluing. Thus, geometrical constructions undergoing smooth deformations and transformation are topologically invariant to each other. For example, a solid sphere can be revolved into a disc by compressing along a diagonal axis exhibiting topological invariance. Nevertheless, the same solid sphere shares a different topology from

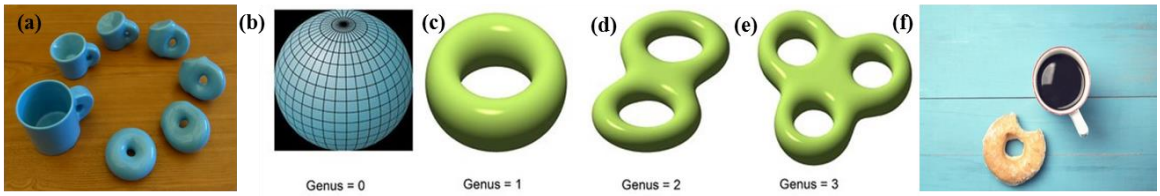

Figure 1.1: (a) Schematic representation of topology showing smooth deformation from cup to doughnut. (b-e) Are representing genus numbers for different topological systems. (f) Shows that the cut on the doughnut is not changing its Topology [21].

a doughnut-shaped geometry, as it is impossible for them to convert into each other's shape by only stretching and bending. Thus, one of the fundamental concepts in topology is to categorize objects by counting the number of holes they enclose. To construct a more formal definition, we use the value of genus (g) given by the Gauss-Bonnet theorem [21]. In mathematics, this theorem connects the curvature (geometry) of the surface to its topology and correlates it to the genus of the object as,

$$\oint^{0}_{\substack{closed \\ surface}} (K.dA) = 4\pi(1-g) \tag{1.1}$$

Where K specifies the Gaussian curvature for a sphere with radius r as; $= {}^{1}/_{r^2}$. Here, g signifies the value of the genus related to the number of holes enclosed in an object. In Figure 1.1 (b-e), we have shown objects with different genus values (same as the number of holes), representing different topological classes. Geometries consuming an equal number of holes are topologically equivalent.

In a band insulator, such a smooth deformation is similar to the modification in the Hamiltonian of a many particles system without closing the bulk band gap. Two quantum states are said to be topologically equivalent only if a smooth transformation occurs from one state to the other without shutting the band gap. Hence, they are topologically similar if the insulators can constantly transform into one another without closing the energy gap.

Another mathematical term, Chern number, η, is also a topological invariant like genus number, and it distinguishes the two states in topologically protected materials. Figure 1.1 (f) shows some exterior cuts on the doughnut, though the no of holes enclosed in the shape is still one evidencing the topology is protected against such deformation. Likewise, the topological surface state is robust against chemical substitution or any external disruption until it affects the topology. However, to describe it, we can define a Berry curvature in the Brillion zone in place of a Gaussian curvature defined in equation (1.1). The surface integral of Berry flux F_m can be expressed as [8]:

$$F_m(K) = \nabla_k \times A_m(K) \tag{1.2}$$

Berry phase, which is correlated to the Bloch wave functions ($|u_m(K)>$, where K represents the momentum), can be used to explain the Chern invariant physically. When K is transported around a closed loop $|u_m(K)>$, it gets a Berry phase which may be expressed by the line integral:

$$A_m = i\langle u_m|\nabla_k|u_m\rangle \tag{1.3}$$

Berry flux surface integral is one way to put it:

$$F_m(K) = \nabla \times A_m(K) \tag{1.4}$$

The total Berry flux in the Brillouin zone is the Chern invariant and may be expressed as:

$$\eta_m = \frac{1}{2\pi}\int d^2k\, F_m(K) \tag{1.5}$$

Here η_m represents a quantized integer. If η = 0, an insulator is considered trivial; if η = 1, it is a quantum spin Hall insulator. A trivial insulator, for η=0, has a gapped edge, whereas a quantum spin Hall insulator with η=1 has a pair of gapless helical edge states, carrying

the electrons having opposite spins. Hence, the edge is conducting for this system unlike the trivial insulator.

1.3 Preservation of Time Reversal Symmetry

Time reversal symmetry is a fundamental phenomenon to be conserved in topologically protected systems. The concept of symmetry comes with the perception associated with the phases of matter through a phase transition. For example, we get liquid crystals by breaking translational symmetry, which the Landau phase transition theory can explain. Furthermore, we can achieve other complex phases such as ferromagnetic (FM) phase braking rotational symmetry and superconducting (SC) phase with broken gauge symmetry. In contrast, for the topologically invariant phase, preserving time reversal symmetry is a must to protect the topological surface state. The TRS protects the TSS against non-magnetic impurities and imperfections, diminishing the possibility of electronic backscattering. In the presence of such robust TSS driven by strong spin momentum locking, the electrons can move only in the forward direction. The electrons can propagate along a backward direction if and only if the electron spin flips its direction. This behavior is because the electron spin is exclusively locked with its momentum vector.

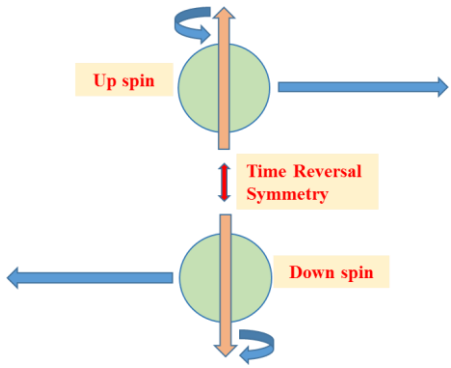

Figure 1.2: Schematic diagram of motion of two electrons having opposite spins with preservation of TRS in TSS.

As a result, electrons having opposite spin configurations follow reverse pathways, as exhibited in Figure 1.2. However, with respect to an observer, these two incidents are identical with reversed directions.

1.4 The Concept of Topology Initiated by Quantum Hall Effect

Before the discovery of the quantum Hall phenomenon, different states of matter related to atoms and their electrons were categorized in the domain of quantum materials using the principle of broken symmetries. All the systems like crystalline solids, magnetic materials, and superconductors are examples of violating translational, rotational, and gauge symmetries, respectively. Nevertheless, as the first condensed matter system without spontaneous violation of any symmetry, the concept of the quantum Hall state and the quantum spin Hall state arrived with the preservation of topological properties. The properties of such matters depend on their topology, and they are topologically distinct from the formerly familiar states of matter. Hence, the concept of the topological phase of matter originated from the theory of the quantum Hall effect, which is the quantum version of the classical Hall effect. Edwin Hall discovered the classical Hall effect in 1879 [22], according to which, ideally, the transverse resistivity in a conducting system exhibits linear dependence with the applied out-of-plane magnetic field. Because under a transverse electromagnetic field, the charge carriers in a metal experience Lorentz force resulting accumulation of equal and opposite charges on the opposite surfaces of the conductor. Thus, the transverse Hall voltage (V_H) is initiated by this phenomenon, as shown in Figure 1.3 (a). Systematic analysis of the Hall effect provides information about the type of charge carriers along with typical values of charge carrier density and charge carrier mobility of the respective system. R_H represents the Hall coefficient *as*:

$$R_H = \frac{zV_H}{I_x B} = \frac{1}{n_e} \tag{1.6}$$

Here, z is the thickness of the conducting bar; I_x represents the current flowing through the system; B is the out-of-plane applied magnetic field; V_H is Hall voltage; n is exhibiting the charge carrier density of the electric charge.

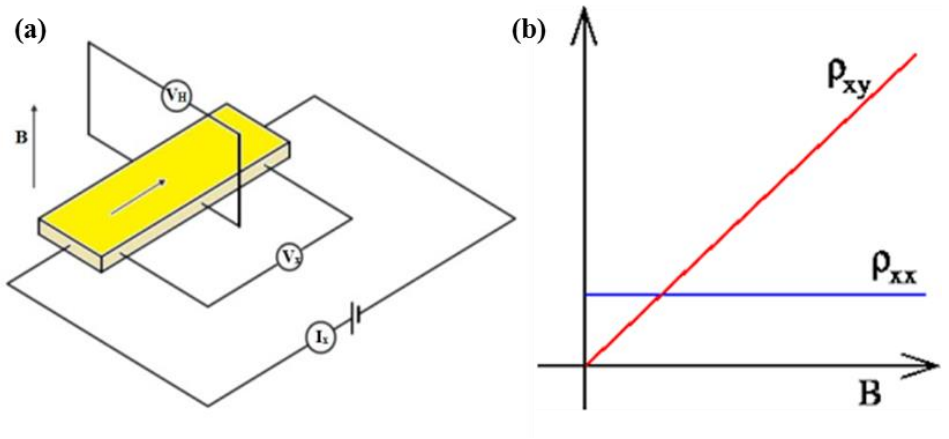

Figure 1.3: (a) Schematic diagram of the Hall effect. (b) Variation of resistivity with the applied magnetic field for classical Hall effect [23].

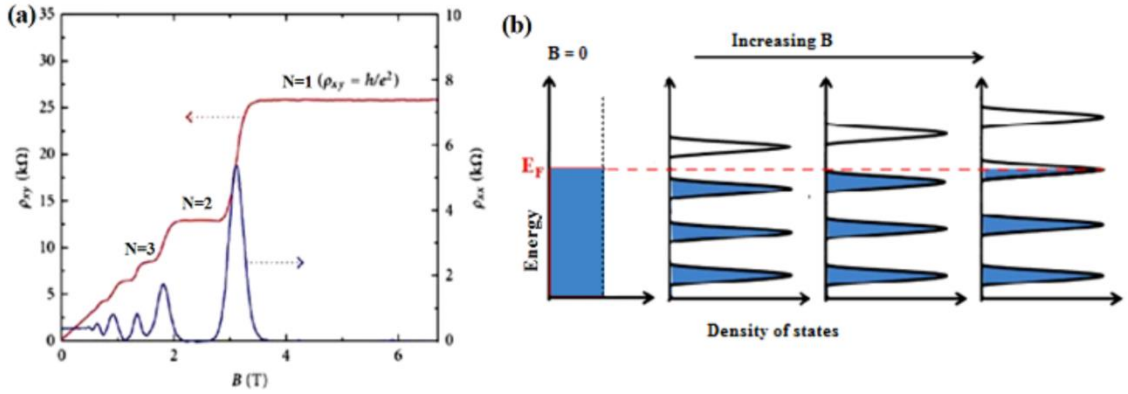

Figure 1.4: (a) Longitudinal (ρ_{xx}) and transverse resistivity (ρ_{xy}) variation with applied magnetic field, revealing the integer quantum Hall Effect at a very low temperature. (b) Quantization of energy level in discrete Landau Levels with the application of magnetic field by increasing magnetic field strength, only those Landau levels that lie below the Fermi level are occupied [24].

Nonetheless, Von Klitzing first discovered the quantum Hall effect in 1980 with the application of a transverse magnetic field on a 2-D electron gas system (2DEG) at very low temperature, a century after the first discovery of the Hall effect, and later awarded with the noble prize in 1985 [3], [4]. Under a perpendicular magnetic field, the electrons are localized and stacked inside the system exhibiting insulating behavior as the bulk state.

However, at the edges (for 2-D), the electrons cannot complete full circles and skip through the edges, creating semi-circles revealing conducting edge states at certainly low temperatures and high magnetic fields. Thus, unlike the classical hall effect where the transverse resistivity (ρ_{xy}) displays a linear dependency with the applied magnetic field (as shown in Figure 1.3 (b)), for QHE, the transverse resistivity is quantized (shown in Figure 1.4 (a)) as:

$$\rho_{xy} = \frac{h}{Ne^2} \tag{1.7}$$

Where *N* is an integer, h is the Plank constant, and e is the electron's charge. Due to the quantization of electronic motion in the cyclotron orbit, the energy levels are also quantized as the Landau levels, as displayed in Figure 1.4 (b). The energy of Landau levels can be expressed as:

$$E_n = \left(N + \frac{1}{2}\right) \hbar\omega_c \tag{1.8}$$

$$\text{Where, } \omega_c = \frac{eB}{m} \tag{1.9}$$

Here *N* is an integer, *B* is the perpendicular magnetic field, and *m* is the electronic cyclotron mass. As shown in Figure 1.4 (b), the Landau levels below Fermi energy (E_F) are occupied (valance band), and the levels above E_F are empty (conduction band) at an absolute zero temperature and in the absence of a magnetic field. However, when we apply some transverse magnetic field, the Landau levels shift upward. At a certain condition, the E_F is situated between two Landau levels when there is a finite separation between the occupied and unoccupied states, similar to the band gap in an insulator. Nevertheless, the situation changes when the E_F lies inside a Landau level without exhibiting a band gap like a conductor. This phenomenon is reflected in the magnetic field dependency of the longitudinal resistivity (ρ_{xx}) (Figure 1.4 (a)), showing metallic and insulating behavior

periodically with quantization of ρ_{xy}. This QHE is a quantum mechanical aspect that initiates the evolution of various quantum phases of matter in quantum materials with the perception of topology.

1.5 Quantum Spin Hall Effect (QSHE)

In continuation to our previous section, if we consider two identical replicas of quantum hall systems situated at the same position under the application of equal and opposite out-of-plane magnetic field (Figure 1.5 (a)), it is possible to nullify the net magnetic field. However, there may still exist some spin-polarized current. After the discovery of such a hypothetical phenomenon, many theories were developed suggesting different systems possessing similar properties in the absence of an external magnetic field. Finally, Kane and Mele proposed the quantum spin Hall effect model in 2005 based on the concept of QHE [25]. They enlightened on the topologically protected systems in which such property can be aroused without applying an external magnetic field, merely driven by the internal spin-orbit coupling protected by the TRS. Preserving the time reversal symmetry, the spin up and spin down in the system follow identical but opposing courses at the edges, which are mutually exclusive to each other, as exhibited in Figure 1.5 (b). Such a QSHE system behaves practically similarly to the hypothetical model of a two-quantum hall system, as shown in Figure 1.5 (a). Noticeably, in QHE, the TRS is broken due to the application of the external magnetic field.

However, in QHSE, the TRS is protected, as no external field is required. Internal spin momentum locking provides the required perturbation to achieve such a phenomenon, distinguishing the QSHE from the QHE. Further, the band structure (energy–momentum diagram) corresponding to a QHE system displays an insulating bulk band gap with the conducting edge state driven by the skipping orbital motion of electrons, as shown in Figure

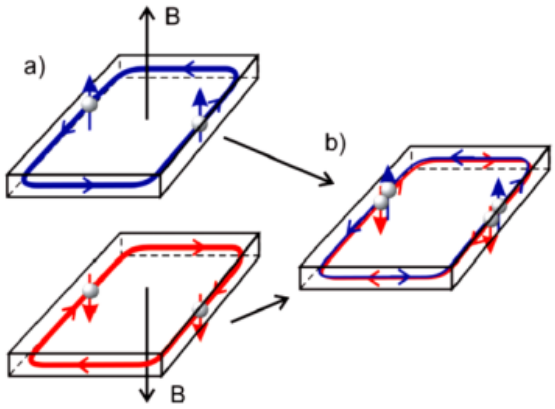

Figure 1.5: (a) Two copies of a QHE edge state for an opposite magnetic field. (b) An amalgamation of these two QHE states creates a quantum spin Hall state without a magnetic field [7].

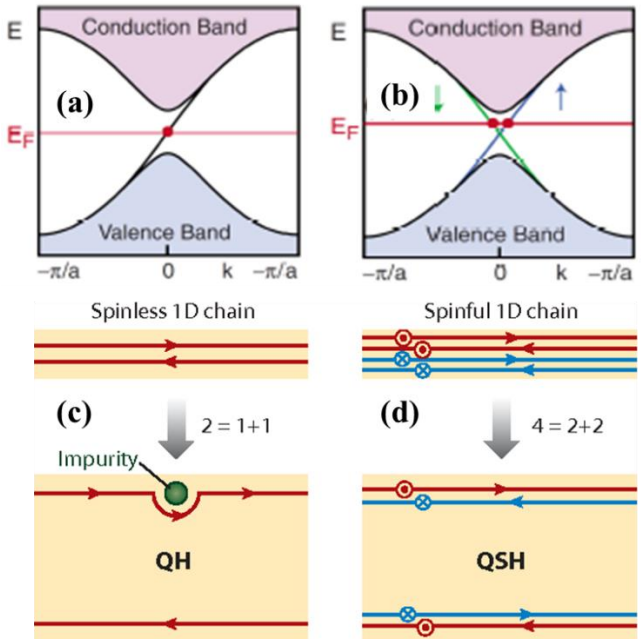

Figure 1.6: (a) Band structure corresponding to QHE and (b) SQHE are exhibited here [4]. (c) QHE with both right-moving and left-moving edge states that are robust against backscattering. (d) QSHE with upper state right moving spin up and left moving spin down. Backscattering is suppressed from non-magnetic impurities [26].

1.6 (a). Whereas, in QSHE, up and down spin of electrons exhibit both left and right moving paths protected by time reversal symmetry, and the edge states corresponding to them demonstrate a Dirac cone ideally at the Fermi surface as shown in Figure 1.6 (b).

Additionally, if we consider the one-dimensional motion of electrons along forward and backward directions, their paths may interfere due to random scattering leading to

resistance. So, to avoid such random collisions, spatial separation between the counterflow directions is needed following a basic traffic control. Here comes the essence of the QHE in the quantum materials controlling the traffic to rule out the scattering effect. Thus, in QHE, the electrons are spatially separated in two mutually exclusive pathways at two opposite edges of the system, as shown in Figure 1.6 (c). So, the symbolic equation shows that the fundamental degrees of freedom are also spatially separated in a QH bar, "2 = 1 (forward mover) + 1 (backward mover)." Noticeably, the states are robust in the sense that the spin-polarized edge states corresponding to the left and right moving electrons remain unaffected from scattering even with the presence of non-magnetic impurity. The propagating electron is prohibited from backscattering and follows a path enclosing around the impurity due to the topological protection [9], as seen in Figure 1.6 (c). Such robust dissipationless transport may serve the spintronics and semiconductor device industry when we overcome the necessity of a large magnetic field as in the QHSE system. However, Figure 1.6 (d) exhibits a spinful 1D system containing four basic channels without applying an external field. In a QSHE system, these channels are spatially divided into separate traffic lanes while maintaining the TRS by means that each edge has a right mover with an upward spin and a left mover with a downward spin, as shown by the symbolic equation "4 = 2 + 2." For QHSE, backscattering is forbidden for both the left and right movers. To elaborate on this mechanism, Xiao-Liang Qi provided a basic analogy regarding the antireflecting coating in most eyeglasses and lenses [9]. The reflected light from the top and bottom surfaces interferes destructively, leading to perfect transmission (shown in Figure 1.7 (a)) modulated by the optical wavelength and coating dimension. Similarly, an electron may reflect by any impurity present in the system and can interfere with other electron reflection paths either destructively or constructively. If the impurity is non-magnetic, the electrons with a clockwise or anticlockwise path turn around the

impurity rotating the spin by an angle 2π under TRS protection. Thus, such electron paths always interfere destructively, resulting in perfect dissipationless transmission, as displayed in Figure 1.7 (b). However, in the presence of a magnetic impurity, TRS is violated. As a result, the backscattered electrons no longer interfere destructively with each other. Physically, with an even number of forward channels, dissipation exists, so the robust edge state in QSHE preserves only with the odd number of forward or backward mover electrons. The QSHE was predicted theoretically and probed experimentally in 2-D HgTe quantum wells with strong SOC [27], [28]. Then this effect was observed in conventional TIs like BiSb alloys, Sb_2Te_3, Bi_2Se_3, and Bi_2Te_3 bulk crystals [29]–[31].

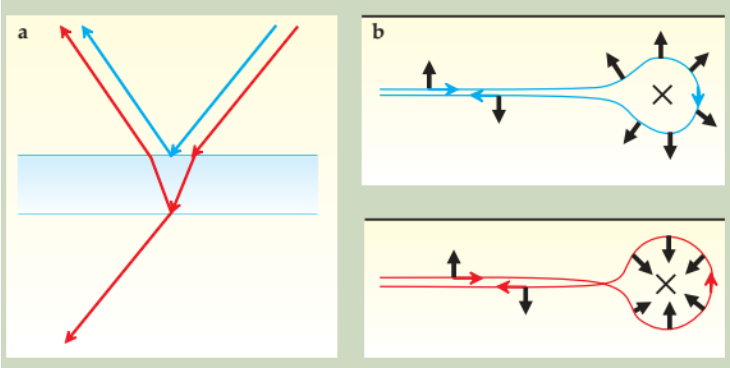

Figure 1.7: (a) Light waves that are reflected by the top (blue line) and bottom (red line) surfaces of a lens with an antireflection coating interfere destructively, suppressing reflection. (b) Schematic diagram of two opposite scattering paths around an impurity for the QSH state. The 2π total path difference between them results in the suppression of Fermion backscattering [13].

1.6 Anomalous Hall Effect (AHE) to Quantum Anomalous Hall Effect (QAHE)

In non-magnetic materials, the Hall voltage is proportional to the applied magnetic field due to Lorentz force, as discussed earlier in detail. The slope of the curve displays linear field dependence and is governed by the type of charge carriers and their density. After discovering the ordinary Hall effect (OHE) (Figure 1.8 (a)), Hall carried out the same experiments for the ferromagnetic materials and observed an unusual change in slope at a low magnetic field. Later, such unusual behavior was found to be originated due to

spontaneous magnetization in the ferromagnetic materials and was recognized as an anomalous hall effect, as shown in Figure 1.8 (b). The internal spin-orbit coupling may play a significant role behind such an anomaly, though the exact reason is still under discussion. Other probable reasons include skew scattering or side jump of carriers (extrinsic mechanisms) and some other intrinsic mechanisms, which may also be responsible for AHE

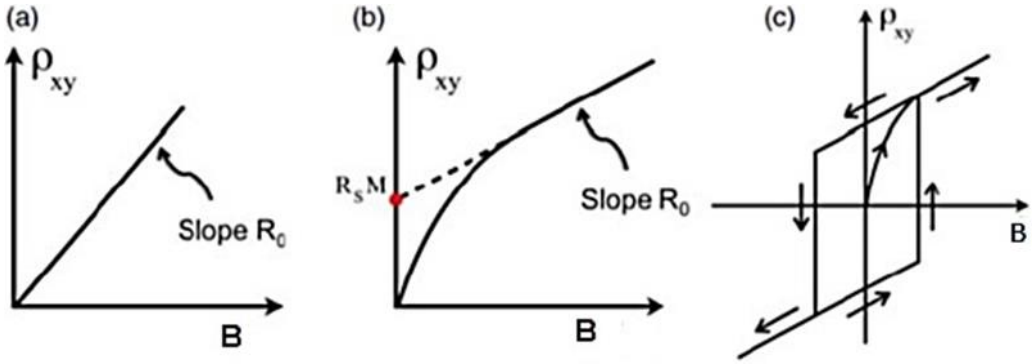

Figure 1.8: The variation of Hall resistivity ρ_{xy} with the applied magnetic field B. (a) Ordinary Hall effect (b) Anomalous Hall effect (c) Measured hysteresis loop from quantum anomalous Hall effect [32].

[32]. The quantum mechanical version of the anomalous Hall effect is known as the quantum anomalous Hall effect. Soon after discovering the quantum anomalous Hall effect, it was realized that the theory used to explain the QHE might be used in explaining QAHE in magnetic quantum materials.

All six members of the hall effect family have already been described in sections 1.4, 1.5, and 1.6. They have been summarized in the following section to compare them in short, as shown in Figure 1.9 (a-f). Here, OHE, AHE, and SHE exhibit classical mechanisms, and QHE, QAHE, and QSHE are the quantum mechanical version of them. For OHE and QHE, an external magnetic field is required along the out-of-plane direction. AHE and QAHE occur in magnetically ordered materials; thus, no external magnetic field is needed. However, due to the presence of an external or internal magnetic field, the TRS is broken for all four systems OHE, AHE, QHE QAHE. Here comes the SHE and QSHE

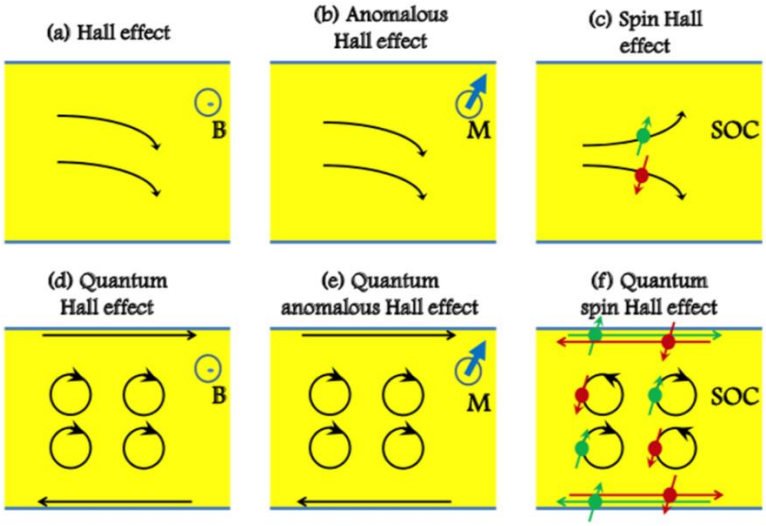

Figure 1.9: The schematic diagram to compare the six members of the Hall effect family as (a) ordinary Hall effect, (b) anomalous Hall effect, (c) spin Hall effect (SHE), (d) quantum Hall effect, (e) quantum anomalous Hall effect, and (f) quantum spin Hall effect [33].

with TRS protection with SOC. All the quantum mechanical systems are topologically identical and different from each other. However, the QSHE is the pioneer of topologically invariant quantum materials and TRS preservation.

1.7 Spin-Orbit Coupling Initiating Band Inversion Mechanism

The spin-orbit coupling has been mentioned several times to describe the topological properties in previous sections. Here I will discuss what it means and why it is so important for quantum matters. When the electron spin and its intrinsic angular momentum interact with its orbital angular momentum, the SOC arises. On the other hand, we can say that the spin up and spin down electrons encounter at the TSS in alternate effective fields, leading them to transmit in the reverse direction. This phenomenon is known as spin momentum locking and is valuable from the application point of view as a data storage and switching device application because this prohibits electron motion from backscattering. If a spin-up electron is locked with its momentum and propagates in the forward direction, backscattering may occur only if the spin flips to the opposite direction,

which is impossible under TRS. However, backscattering can occur if TRS is broken (in case of magnetic impurity or applying an external magnetic field). Thus, the SOC and TRS both preserve the robustness of TSS and do not allow backscattering. Generally, the s and p orbital electrons initiate the conduction and valence bands in ordinary semiconductors where the conduction band (s-band) shifts upward, and the valance band (p-band) shifts downwards [9]. Therefore, these bands never cross each other in ordinary materials. However, the presence of strong SOC initiates a band inversion in topological materials (mainly TIs), which is accountable for the unique properties. Here, due to strong SOC in heavy metals, the p-band (valance band) shifts upward and the s-band shifts downward direction. Due to this band shifting, the s and p bands cross each other, and the normal band structure gets inverted, called band inversion [34], [35]. Hence, due to band inversion, the p-band energy becomes higher than the s-band. The points where the bands intersect each other introduce the surface state overcoming the bandgap. For example, we studied the orbital splitting in the atomic energy levels of a conventional topological insulator Bi_2Se_3 and displayed it in Figure 1.10 [30]. The energy level shifting and splitting may happen fundamentally due to chemical bonding, crystal field splitting, and spin-orbit coupling. The unit cell of Bi_2Se_3 consists of two Bi and three Se atoms, and the outermost configuration of Bi and Se atoms are $6S^2\ 6p^3$ and $4S^2\ 4p^4$, respectively. Hereby, the outermost cell of each atom contains three p orbitals as p_x, p_y and p_z. Therefore, there are total fifteen p orbitals in a unit cell of Bi_2Se_3. As shown in Figure 1.10, in stage I, Bi energy levels are pushed up, and Se levels are pushed down because of chemical bonding. In stage II, due to crystal field splitting Bi energy level splits into two levels with one odd and one even parity denoted as $P1^-_{xyz}$, $P1^+_{xyz}$, respectively. In contrast, Se energy level splits into three states with different parity i.e., two odds, one even denoted as $P0^-_{xyz}$, $P2^-_{xyz}$ and $P2^+_{xyz}$, respectively. In stage

III, strong SOC leads to band inversion in the Bi_2Se_3 system as the energy level below the E_F moves to the upside, and the level above the E_F moves downward.

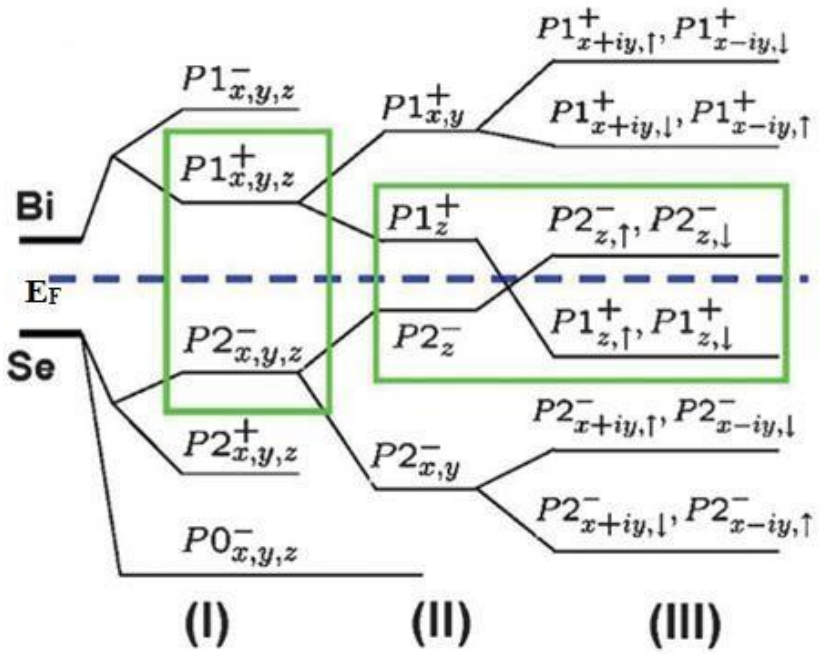

Figure 1.10: Schematic picture of the band inversion of Bi and Se p orbitals in Bi_2Se_3 at the Γ point. Stage I represents the effect of chemical bonding, Stage II represents the crystal field splitting, Stage III represents the effect of SOC [9].

1.8 Weak Localization (WL) and Weak Antilocalization (WAL) Effects

Weak antilocalization is a phenomenon associated with the TSS describing the localization and delocalization of electrons in the system. WAL originated from π Berry phase generally appears at very low temperatures under the application of a small magnetic field resulting in a destructive quantum interference between time-reversed loops created by scattering trajectories [9], [36]. The destructive interference can prevent the backscattering of electrons. As a result, the value of conductivity increases with decreasing temperature due to the reduction in decoherence mechanisms at low temperatures. The interference and conductivity can be destroyed by applying a magnetic field. Therefore, the signature of WAL is a negative magnetoconductivity which can be easily observed in many topological materials. It has been realized that large spin-orbit scattering in some materials

may proceed a crossover in quantum interference from destructive to constructive with varying temperatures and magnetic fields. The electrons are localized in the conductors due to constructive interference between two time-reversed paths of the electron wave function, reducing their ability of current transport exhibiting the WL effect. In 1980, Hikami, Larkin, and Nagaoka (HLN) [37] analyzed the WAL effect for 2-D systems at very low temperatures and small magnetic fields. The HLN equation can be expressed as [38]–[41]:

$$\Delta G(B) = G(B) - G(0) = \frac{\alpha e^2}{\pi h}\left[\psi\left(\frac{1}{2}+\frac{h}{8\pi e B l_\varphi^2}\right) - ln\left(\frac{h}{8\pi e B l_\varphi^2}\right)\right] \qquad (1.10)$$

Where l_φ represents phase coherence length, ψ is a digamma function and $A = \frac{\alpha e^2}{\pi h}$ represents the no. of the conduction channel, and α is the prefactor value.

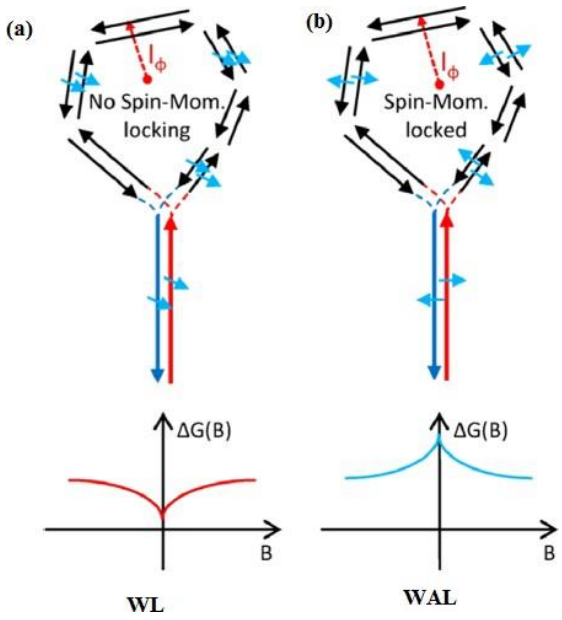

Figure 1.11: (a) The two time-reversed scattering loops without spin-momentum locking exhibiting weak localization in magnetoconductivity (ΔG (B)). (b) The two time-reversed scattering loops with spin-momentum locking exhibited weak antilocalization in ΔG (B) [13].

Further, the bulk state (3-D) of TIs may demonstrate the WAL effect with quantum correction at low fields similar to the surface state. However, TI bulk state comprises a finite gap which generally leads to the WL effect. Also, the WAL behavior diminishes with

the implementation of the magnetic field. Therefore, the consistent quantum correction to the bulk state conductivity is given by [42]–[44]:

$$\Delta G(B) = -\frac{e^2}{2\pi h}\left[\psi\left(\frac{1}{2}+\frac{B_\Phi}{B}\right) - ln\left(\frac{B_\Phi}{B}\right)\right] + \frac{3\alpha e^2}{2\pi h}\left[\psi\left(\frac{1}{2}+\frac{B'_{so}}{B}\right) - ln\left(\frac{B'_{so}}{B}\right)\right] \quad (1.11)$$

The above-written quantum interference effect (QIE) formula consists of two contending contributions describing the field-dependent crossover from WAL to WL phenomena. The first term explains the WAL effect at the lower fields, and the rest is accountable for the WL effect at relatively higher magnetic fields [43], [45]. Here,

$$B_\Phi = \frac{h}{8\pi e l_\varphi^2} \quad (1.12)$$

$$B_{SO} = \frac{h}{8\pi D e \tau_{so}} \quad (1.13)$$

$$B_e = \frac{h}{8\pi D e \tau_e} \quad (1.14)$$

$$\text{And } B'_{SO} = \frac{4}{3}B_{SO} + B_\Phi \quad (1.15)$$

Here, τ_{so} is the spin-orbit scattering time and τ_e is the elastic scattering time. Hence, τ_φ is considered as electron dephasing time with a relation, $l_\varphi = (D\tau_\varphi)^{1/2}$. Here, D represents the diffusion constant.

1.9 Quantum Materials

The basic mechanisms of quantum materials have already been discussed in the previous sections; now, the classification of such materials as topological insulators, Weyl semimetals, superconductors, and quantum spin liquid, Graphene, spin ice systems are well-known in the world of quantum materials. These materials possess different shapes and compositions but share a common thing: electron confinement, which occurs along one or more directions and causes mysterious properties in such systems. The geometrical

constraints of these systems drive electrons to act collectively instead of independently. As a result, a bunch of electrons may behave like a quasi-particle and originates different fascinating properties like superconductivity, the development of mass-less fermions, or the apparently impossible single pole magnets. In particle physics, recent research has developed some familiar quasi-particles predicted by complex theories practically by the large hadron collider overcoming all the difficulties. However, quantum materials open new prospects to explore fundamental as well as applied material science. The topological current in quantum materials is meant to serve the future generation of spintronics with nonreciprocal responses based on the generalized current transmission, i.e., information. Topological protection provides dissipationless robust quantum states making such materials useful in magnetoelectronic integrated circuits, high-density storage devices, and quantum computing which may contribute to future energy and information technologies. Therefore, I am intended to introduce the historical development of some physically existing quantum materials like 2-D and 3-D topological insulators, Weyl semimetals, and Skyrmions, along with their structures and intriguing properties. Indeed, these materials pave the way for next-generation quantum electronic and computational technologies.

1.9.1 Topological Insulators

As described in the previous section, topological insulators are widely studied quantum materials with an insulating bulk and a conducting surface (edge) state. The surface states are quite different from the ordinary conducting states where electrons with opposite spins are distributed over a Fermi surface with spin degeneracy. These surface states are topologically invariant, and this phenomenon is made possible by the two important features in quantum mechanics, which are:

1. symmetry under the reversal of the direction of time, and

2. spin–orbit interaction that usually occurs in mercury and bismuth-like heavy elements.

However, depending on the properties and dimensionality, the TIs can be classified into two categories as:

1. 2-D topological insulators
2. 3-D topological insulators

Let us discuss the historical development and intriguing properties of these TIs.

1.9.1.1 2-D Topological Insulators

As discussed earlier, the electrons associated with opposite spins follow identical but opposite lanes at the edges creating spin-polarized currents due to large SOC and preservation of TRS. In 2-D TIs, the electrons follow one-dimensional (1-D) conduction channels having edge states. As a 2-D system, Graphene was proposed as the system that may show the QSHE at the beginning by Kane and Mele in 2005 [25]. However, carbon possesses a very weak SOC. Thus, QSHE could not be observed in Graphene experimentally. Then, the presence of QSHE state in HgTe quantum wells (QW) was predicted by Bernevig *et al.* in 2006 [27]. A thin layer of HgTe is inserted between two layers of CdTe to construct 2-D QW structures that provide a special route to change the compound's electronic structure. The thickness of HgTe plays a significant role in the band structure of this heterostructure [4], [9], [46]. The electronic band structure of this heterostructure at the Γ point has an inverted band structure. The confinement energy increases as the value of d_{HgTe} decreases, due to which the energy band shifts. When the thickness d attains the critical value, i.e., $d = d_c$, QSHE emerges without any external magnetic field. The heterostructure of CdTe/HgTe/CdTe and the band structures of HgTe, CdTe are shown in Figure 1.12 (a). With the variation of the width 'd' of the quantum well,

the corresponding band structure is represented in Figure 1.12 (b). After the critical width d_c, band inversion at the r point occurs, 1-D helical edge state comes to light, and band inversion occurs at the boundaries of the 2-D quantum well. At the critical thickness d_c (6.3nm), the bandgap vanishes, and the Dirac cone touches each other at a point called Dirac point. The QSHE in HgTe quantum well systems has been experimentally verified and reported. The experimental evidence for the spin polarization of the QSH edge state also supports this phenomenon. Soon after this theoretical envision, König *et al.* [28] confirmed it experimentally by observing QSHE in HgTe at 30 mK without the application of an external magnetic field. Therefore, HgTe QW is considered the first 2-D TI. After the experimental validation of QSHE in CdTe/HgTe/CdTe QW, it was also predicted that QSHE may also exist in type II semiconductor such as InAs/Gasb/AlSb, when Fermi level lies in the bulk band gap [47].

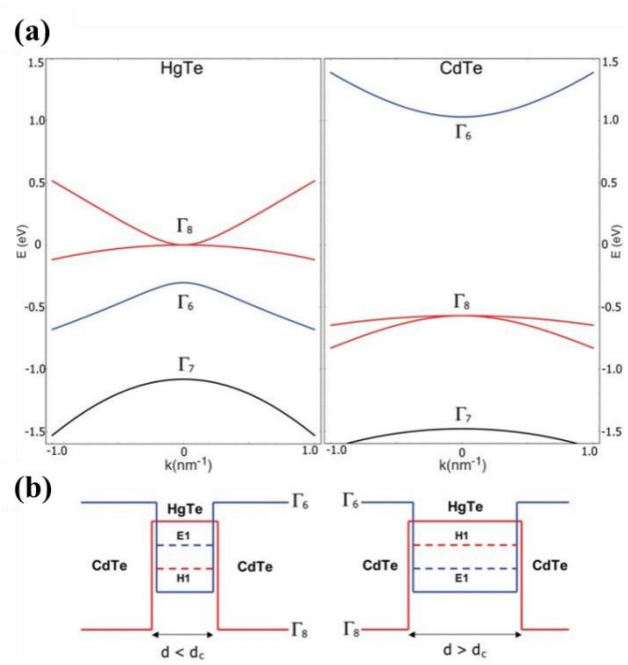

Figure 1.12: (a) Bulk energy bands for HgTe and CdTe at r point (b) CdTe/HgTe/CdTe quantum well in normal regime $d < d_c$ and in inverted regime $d > d_c$ [27].

1.9.1.2 3-D Topological Insulators

After the development of 2-D topological insulators, the concept of 3-D topological insulators was established by Moore and Balents [48], Roy [49], Fu, Kane, and Mele [50]. 2-D topological system contains conducting edge state, whereas 3-D topological insulators comprise conducting surface state with 2-D conduction channel. In 3-D TIs, the surface state's band structure can be described as a 2-D state with a single Dirac cone. Comparison between 2-D and 3-D TIs have been displayed as a schematic in Figure 1.13. Strong topological insulators have an odd number of Dirac cones. 3-D TIs possess four Z_2 topological invariants (υ_0, υ_1, υ_2, υ_3), where υ_0 is associated with strong topological invariant and υ_1 - υ_3 belongs to the weak topological invariant. The strong topological insulator $\upsilon_0 = 1$ follows that there must be an odd number of Dirac cones present at the surface of topological insulators. The spin-momentum locking in the perpendicular direction of the surface state is the most intriguing property of the 3-D topological insulators. The state having momentum K and –K possess opposite spins, i.e., up spins propagate in the +ve x direction, and down spins move in the –ve x direction. Therefore, the backscattering does not occur at the surface state of topological insulator and the surface state becomes robust.

Therefore, immediately after the experimental verification of the existence of QSHE in 2-D in HgTe quantum well in 2008, Hsieh *et al.* [52] reported the first experimental evidence of the presence of the 3-D topological state in $Bi_{1-x}Sb_x$. Further, the presence of QSHE in 3-D $Bi_{1-x}Sb_x$ was observed by utilizing the angle-resolved photoemission spectroscopy technique (ARPES) [52]. Soon after the experimental discovery of $Bi_{1-x}Sb_x$, in 2009, Zhang *et al.* [53] predicted some chalcogenide compounds (A_2B_3) as 3-D TI theoretically by using *ab initio* theory. The non-trivial surface state and

calculated bulk bandgap of Sb_2Se_3, Bi_2Se_3, Sb_2Te_3, and Bi_2Te_3 have been shown in Figure 1.14. The band structure can be easily seen in these materials, which are experimentally verified using ARPES. In Figure 1.14, the linear dispersion at the surface state can be

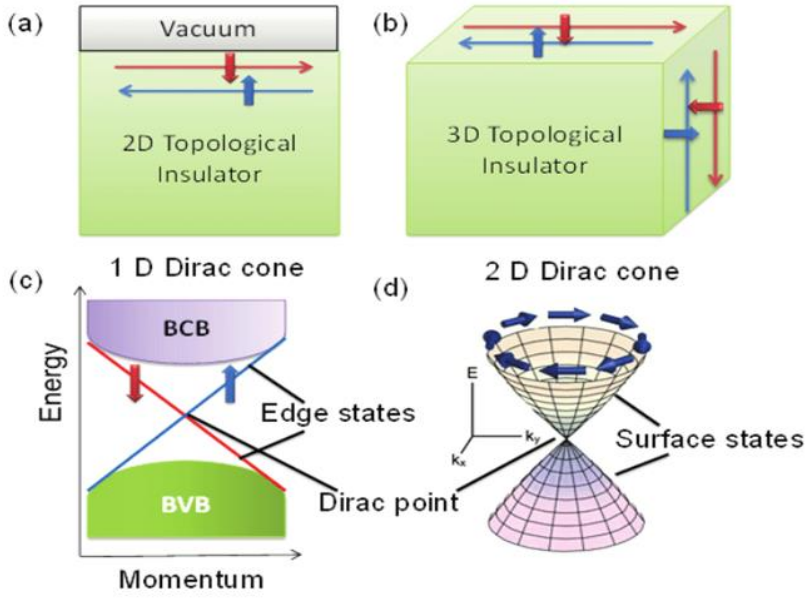

Figure 1.13: (a-b) 2-D and 3-D topological insulators with spin-polarized edge and surface states at the system boundary are shown schematically in real space. (c-d) The development of the 1-D and 2-D Dirac cones is depicted in the energy band diagrams of the 2-D and 3-D topological insulators in momentum space. BCB corresponds to the bulk conduction band, and BVB represents the bulk valence band [51].

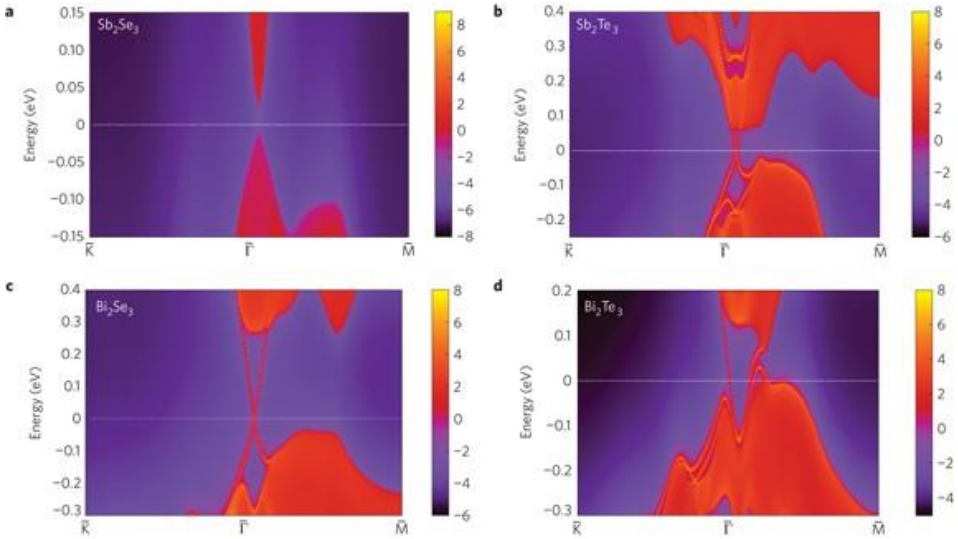

Figure 1.14: Calculated band structure of Sb_2Se_3, Sb_2Te_3, Bi_2Se_3, and Bi_2Te_3 by ab initio DFT. The occupied bulk and surface states have been represented by red, and the blue color signifies the bulk band gap [5].

Seen in the ARPES spectrum of Sb_2Te_3, Bi_2Se_3, and Bi_2Te_3. The presence of Dirac cone in the band structure confirmed it as a TI, and the bulk band gap was calculated as 100 meV for Bi_2Te_3, 260 meV for Sb_2Te_3, and 300 meV for Bi_2Se_3, respectively. Bi_2Se_3, Bi_2Te_3 and Sb_2Te_3 possess topologically protected surface states like $Bi_{1-x}Sb_x$ [5], [54]. These topological materials are easy to prepare as pure phase single crystals in 3-D and also can be grown as 2-D thin films in a perfect environment. They exhibit topologically protected surface states as 2-D and 3-D, making them the most studied TI system.

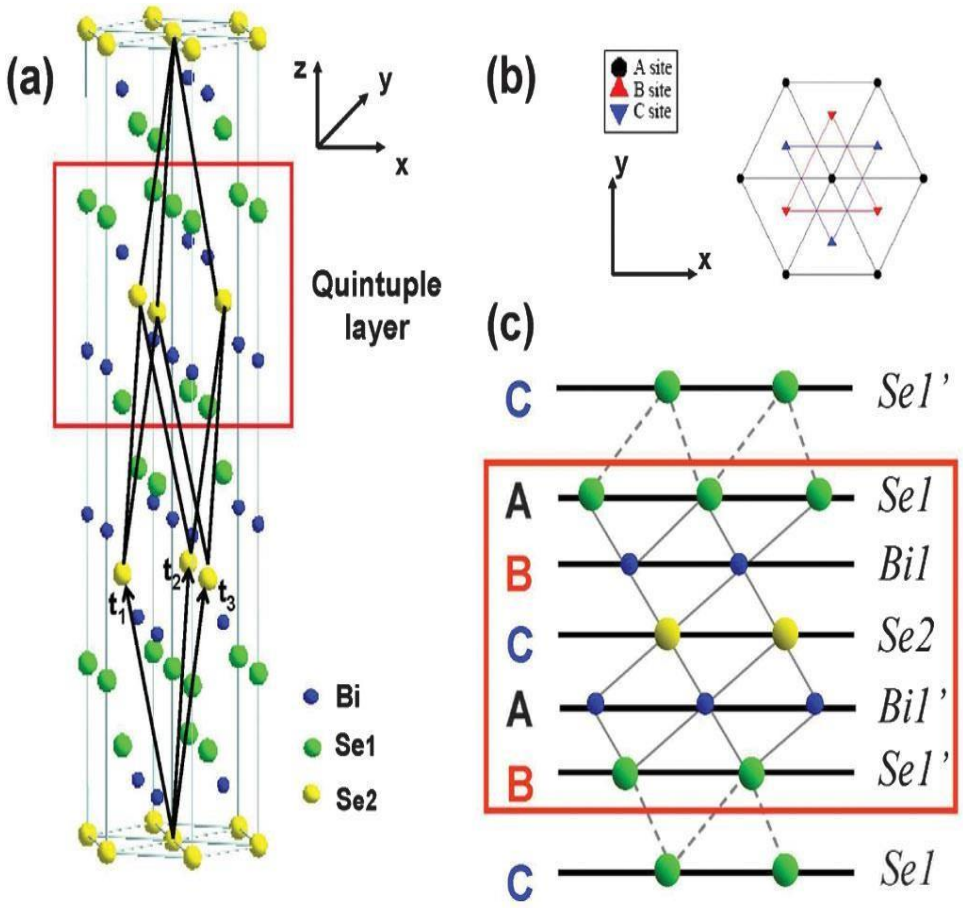

Figure 1.15: (a) Crystal structure of Bi_2Se_3, the red box shows single quintuple layer (b) shows that three different A, B, and C sites are assigned to a triangular lattice in one quintuple layer (c) Se and Bi atoms are arranged in a sequence in quintuple [9].

However, 3-D Bi_2Se_3, Bi_2Te_3, and Sb_2Te_3 are layered materials and belong to the rhombohedral crystal structure with $R\bar{3}m$ space group. Figure 1.15 shows the crystal structure of Bi_2Se_3. The structure contains five atoms per unit cell as Se1-Bi1-Se2-Bi1'-

Se1' along the c-axis, manifesting one quintuple layer. The atomic layers consist of covalent bonds, whereas the weak Van der Waals force exists between two adjacent quintuple layers. The thickness of one quintuple layer is 1 nm. Each layer of atoms makes a triangle lattice known as a tetradymite-type lattice. The triangle layers are ordered A-B-C-A-B-C type arrangement along the z-axis. In one unit cell, there are two Bi atoms and three Se atoms in which two equivalent Bi (Bi1 and Bi1') atoms, two equivalent Se atoms (Se1 and Se1'), and one equivalent Se atom (Se2) are present.

1.9.2 Weyl Semimetals

Weyl semimetals are a class of quantum materials possessing a topological phase of matter and are regarded as an intermediate state between metal and insulators. These semimetals are quite different from the topological insulators and can be considered as 3-D analogous to Graphene by breaking either TRS or inversion symmetry (IS). In WSM, the valence and conduction bands touch each other in bulk at certain points. These linear-dispersive band-crossing points in bulk are called Weyl nodes. These Weyl nodes act as a magnetic monopole in momentum space and always exist in pairs. The charge of the Weyl node is associated with the Berry flux in the momentum space. It has been manifested that the charge associated with Berry curvature in band structure must be zero; hence there must be an even number of Weyl nodes overall. The Weyl nodes projection on the surface Brillouin zone is connected by an open line surface state called the Fermi arc, as displayed in Figure 1.16 (a) [55]. The low-energy bulk excitations of Weyl semimetal are Weyl fermions. The transport by such types of excitations in the materials is fascinating due to its unique properties and potential applications. Thus, the WSM surface state is depicted as the Fermi arc at the Fermi surface, which differs from the TIs. Hermann Weyl proved that a massless fermion exists in the Dirac equation in 1929 [56], which was later called the

Weyl fermion. Except for neutrinos, which have chirality, all fermions in the standard model are Dirac fermions. In a Weyl semimetal, Weyl Fermions exist as a low-energy excitation, in which electronic bands diffuse linearly along the three-dimensional momentum space from a node known as a Weyl point. WSMs are associated with a lack of time-reversal or inversion symmetry. These Weyl points act as topological charges, sources (+ chirality), and sink (- chirality) of Berry curvature. The topological entanglement between conduction and valence bands, which is analogous to a magnetic field in the momentum space, can be described by a quantity called the Berry curvature. If these Weyl points are not present in pairs, the Berry flux diverges. Topological Fermi arcs are likely to arise on the 001 surface, linking the opposing chirality projections of the W_1 and W_2 Weyl points, as illustrated in Figure 1.16 (b, c). Because they are both compressed into the thin surface gap between the projected bulk electron and hole pockets, surface Fermi arcs are difficult to distinguish experimentally from trivial surface states or projected bulk states. A topological Fermi arc on the Fermi surface has been shown in Figure 1.16 (a) and (b) for a conventional Weyl semimetal.

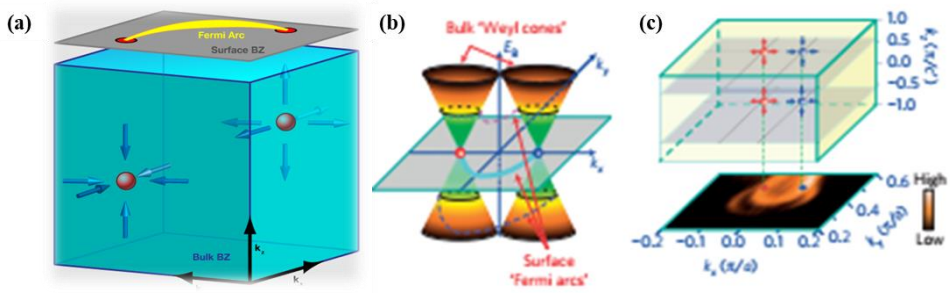

Figure 1.16: (a) Schematic diagram of Weyl semimetal showing Fermi arc as the surface state. (b) Surface projection of a pair of Weyl cones connecting the Fermi arc. (c) Location of experimentally determined Weyl nodes in the 3-D Brillouin zone and their surface projection [17].

1.9.3 Skyrmions

Another eminently relevant and auspicious discovery in the field of topological matter is the magnetic Skyrmion. After the phenomenal discovery of Skyrmions by Tony Skyrme (1960), magnetic Skyrmions were discovered in the chiral magnet MnSi [57]. Skyrmions are evidenced to be adequately advantageous over domain wall memory devices considering the requirement of a small electrical excitation current to transmit an equivalent amount of information [58]. Eventually, Skyrmions represent topologically protected field configurations with particle-like characteristics providing enormous stability even at the nanoscale. Figure 1.17 shows different types of magnetic configurations classified as Skyrmions. Such vortex-like whirling nano-object in non-centrosymmetric non-trivial metallic helimagnet displaying topologically invariant spin texture represents it as a potential carrier of information in future high-density data storage ultrafast spintronics and microwave devices. Irrespective of such amusing properties, the utilization of Skyrmions has not been accomplished yet as spintronic devices. There are several shortcomings related to the current-driven motion of such magnetic particles and the restricted region of Skyrmions phase-space (*H*-*T*).

The origin of Skyrmions is based on four simple mechanisms: 1) long-ranged magnetic dipolar interaction, 2) Dzyaloshinskii-Moriya interaction (DMI), 3) Frustrated exchange interaction, 4) Four-spin exchange interaction [59], [60]. DMI modulated Skyrmions emerged with inordinate attention existing with a particular direction of whirling [61]. A Skyrmion introduced material displays the Skyrmion phase at a specific temperature range, which is a compelling property of any Skyrmion-hosting material. The stability of this Skyrmion phase can be well-tuned by different adjusting parameters such as physical, mechanical, and chemical pressure employing uniaxial strain and chemical

substitutions. Meanwhile, competition occurs between the ferromagnetic (FM) exchange and antisymmetric DMI resulting a chiral spin helical state appeared periodically below the transition temperature in terms of Curie temperature (T_C) of the specific material [62]. The weak magneto crystalline anisotropy can be used to establish how the spiral propagation vector is oriented, analogous to the high-symmetry crystallographic directions. Degeneracy is induced along the direction of the propagation vector in the cubic system. As a result, a macroscopic sample develops a multidomain helical state, and this is conceivable to consider a Skyrmion as a two-dimensional object trivially sustained along the third dimension. Thus, the multidomain helical state is revolutionized by applying an external magnetic field to a single-domain state. This state starts propagating parallel to the applied magnetic field with a conical spiral [63]. When the Zeeman energy overcomes the DMI energy, the phase converts towards a completely polarized state [64]. In such a system, an extremely small current is required to modify the spin configurations by virtue of the small domain size. As a result, such materials hold great promise for information technology. Subsequently, the challenge is to discover the specific operating region of Skyrmion in the magnetic field (H) - temperature (T) phase space and somehow expand the functional range. The complicated struggle amidst the exchange interaction, DM spin-orbit interaction, and anisotropic crystallinity in a non-centrosymmetric helimagnetic compound develops the field temperature (H-T) phase diagram. This exclusive property enlarges the utilization space of such materials as high-potential information devices, drastic spintronics, and dynamic microwave devices. $Co_3Sn_2S_2$ is a shandite-type compound possessed with Kagome sub-lattices that initiated an unconventional magnetic phase below its ferromagnetic transition temperature. This phase induces a spin state which is non-trivial at low-field H-T phase space [65]. Previously, the implementation of AC susceptibility measurements on the Ni/Fe-substituted $Co_3Sn_2S_2$ compounds was executed to examine the

unconventional magnetic phase under a certain magnetic field to comprehend the consequence of chemical substitution on such compounds [66]. The discovery of such a magnetic Weyl-semimetal exhibiting analogous magnetic domain microstructure triggered the research related to Skyrmionic semimetals [67]. Earlier literature assured the possibility of tuning the stability of the Skyrmion phase in a Skyrmion lattice to a broader and higher-temperature region by the implementation of uniaxial strain [68]–[71], chemical substitution [63], [72]–[75], physical or chemical pressure [59]. Also, a certain magnetic anomaly was presented as a signature of the non-colinear Skyrmionic phenomenon by *H. C. Wu et al.* with the application of a very low magnetic field under physical or chemical pressure. They further depicted an *H-T* phase diagram recognizing the Skyrmion phase in $Co_3Sn_2S_2$ originated by magnetic susceptibility measurement [76]. Such stimulating discoveries introduce the magnetic WSM $Co_3Sn_2S_2$ as a promising applicant in spin-frustrated systems exploring the isentropic and isothermal magnetic moment below the ordering temperature.

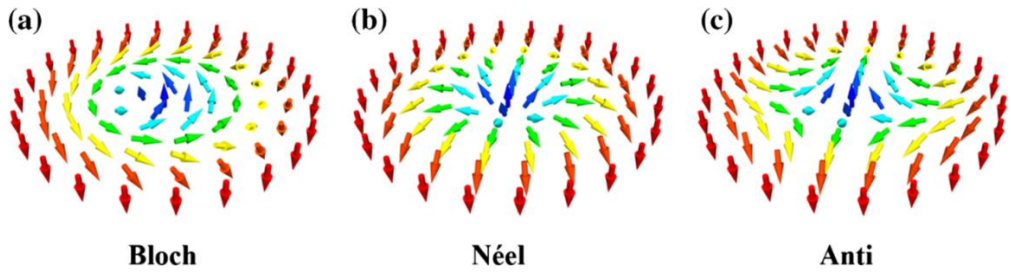

Figure 1.17: Detailed magnetic configurations of (a) a Bloch-type Skyrmion, characterized by a transverse helix with an anticlockwise spin rotation, (b) a Néel-type magnetic Skyrmion, characterized by the anticlockwise-rotated magnetization in a spin cycloid, and (c) a magnetic anti-Skyrmion, characterized by boundary walls that have alternating Bloch and Néel types as one trace around the boundary [77].

1.10 Objective of Present Thesis

In my thesis, my objective is to prepare different quantum materials: topological insulators and Weyl semimetals and to study their basic mechanisms like physical, magnetic, and thermoelectric properties. To do so, firstly, I have chosen some 3-D single

crystalline topological insulators along with a minimal quantity of magnetic impurity to observe their intriguing topological properties. Then, I prepared heterostructures of some primary topological insulators and ferromagnetic materials to observe the magnetic interfacial consequence and how the dimensional confinement affects the topological properties. Furthermore, I planned to prepare a ferromagnetic Weyl semimetal that exhibits a Skyrmion-like vortex magnetic phase at a certain temperature region to enhance its Skyrmion stability and examine its magnetic properties with application of chemical pressure by chemical substitution.